ICAS-98-5,9,2

THE EFFECT OF DAMAGE ON THE PERFORMANCE OF POSTBUCKLING FIBRE COMPOSITE SHEAR PANELS

Rodney S. Thomson[1] and Murray L. Scott[2]

[1] *Cooperative Research Centre for Advanced Composite Structures Limited, 506 Lorimer Street, Fishermens Bend, Victoria, 3207, Australia.*
[2] *The Sir Lawrence Wackett Centre for Aerospace Design Technology, Department of Aerospace Engineering, Royal Melbourne Institute of Technology, GPO Box 2476V, Melbourne, Victoria, 3001, Australia.*

ABSTRACT

The postbuckling performance of three-blade-stiffened carbon fibre/epoxy shear panels containing artificial delaminations has been investigated. The working dimensions of the panels were 250 x 250 mm with 25 mm high stiffeners. The skins of the panels were 1 mm thick consisting of eight plies of uni-directional carbon fibre/epoxy tape, while the stiffeners were 2 mm thick consisting of 16 plies. Static tests under in-plane shear loading showed that buckling initiated at 28 kN (79 N/mm), delamination growth at 48 kN (136 N/mm) before ultimate failure at approximately 60 kN (170 N/mm). An analysis technique to determine the effect of the delamination was proposed based on the virtual crack closure technique. The strain energy release rate around the circumference of the imbedded delamination was determined from a geometric nonlinear finite element analysis using two-dimensional plate elements. The predicted location and mode of delamination growth was shown to agree well with experimental results. Further work is required to be able to predict the actual failure load due to the mixed mode failure experienced.

INTRODUCTION

The progressive introduction of advanced fibre composite materials into primary aerospace structures has enabled significant performance improvements to be achieved. However, the use of composites in stiffened panels has generally been restricted to designs which do not buckle under compression and shear loads for various reasons including some relating to uncertainties associated with their long term durability. In order to improve the relative competitiveness of composites in primary structural applications, this conservative philosophy needs to be reconsidered and postbuckling structures used.

The postbuckling performance of metal panels has been investigated extensively and is relatively well understood. Due to the poor through-thickness properties of laminated composites, likely failure modes include delamination and stiffener-skin separation. In addition, certification requirements for aerospace structures include allowable defects and no growth of defects during the normal operation of the aircraft. Much of the work conducted in the area of postbuckling composite panels has not adequately addressed these aspects.

Experimental and analytical investigations into the postbuckling behaviour of composite shear panels have been undertaken by a small number of researchers. Some significant work has been performed by Weller and Singer[(1)] who investigated the buckling and postbuckling response of unstiffened shear webs and "I" and "J" stiffened panels. The performance of flat, postbuckling, "I" and hat-stiffened composite shear webs was investigated by Agarwal.[(2)] Panhwar et al.[(3)] investigated the performance of flat, unstiffened panels under shear. More recently, Wiggenraad et al.,[(4)] Gadke et al.[(5)] and Greenhalgh et al.[(6)] have investigated the effect of impact damage and delaminations on the performance of stiffened composite panels. It was found that the presence of damage did influence both the global behaviour of stiffened panels as well as the failure mode and load. However, this work did not investigate situations where both the sub-laminate formed by the delamination and the underlying laminate were buckling.

Predicting the effect of damage in a postbuckling stiffened composite structure presents a number of difficulties. Firstly, the behaviour of the structure is very complex and difficult to predict with certainty. The necessary prediction of the stresses or strains to determine the effect of the damage is therefore made

very difficult. Secondly, the orthotropic nature of the material used in the manufacture of the panels makes it difficult to generalise results from one application to another. Thirdly, the type of damage, whether it be matrix cracking, delamination or others, will dictate the approach used in predicting its effect. This study has focussed on the effect of an imbedded delamination on the performance of a postbuckling, stiffened, composite panel loaded in shear. Tests were conducted and analytical techniques developed to predict the location and load level under which the delamination will grow.

TEST METHODOLOGY

Test Specimens

Tests were performed on three-blade-stiffened panels, as shown in Figure 1. The overall dimensions of the panels were 340 x 340 mm with working dimensions of 250 x 250 mm. The integral blade-stiffeners were 25 mm high with run-out angles of 45°. The skins and stiffeners were co-cured in an autoclave using flexible tooling. The material used to manufacture the panels was T300/914C carbon fibre/epoxy, unidirectional, pre-impregnated, zero-bleed tape, the properties of which are provide in Table 1. The skins of the panels were 1 mm thick consisting of eight plies of tape and the stiffeners were 2 mm thick consisting of 16 plies. The clamping regions of the panels were built-up to a thickness of 1.5 mm consisting of 12 plies. The stacking sequences of the panels are detailed in Figure 1. A design criterion was for the stacking sequence of the stiffeners to be symmetrical. As shown in Figure 2, the top four plies of the skin formed part of the stiffener to improve the interface strength, resulting in the lay-up of alternate bays of the skin not being symmetric. The panels were trimmed and drilled to the geometry shown in Figure 1 and inspected using through-transmission, ultrasonic C-Scan to detect manufacturing flaws.

Previous studies by the authors have been concerned with the performance of undamaged panels.[7] To assess the effect of damage, the panels for this study were manufactured with a 50 mm diameter piece of teflon film imbedded in the lay-up in the centre of the panel. The location of the film in the stacking sequence is shown in Figure 2. This situation is representative of a delamination introduced during manufacture or resulting from in-service damage. The presence and location of the inserts was verified by C-Scan of the panels.

Test Procedure

Panels were tested in a "picture frame" shear fixture with anti-slip strips placed between the panel and the rig edge members to achieve effective load transfer through frictional contact. The panels were fitted with three-element strain gauge rosettes, located front and back at various locations on the panel (Figure 1). A linear variable differential transformer (LVDT) was employed to measure the out-of-plane displacement of a buckle peak during the tests. The shadow moiré interferometry technique was also used to qualitatively correlate the buckle shapes and out-of-plane displacements with those obtained through analytical techniques.[7]

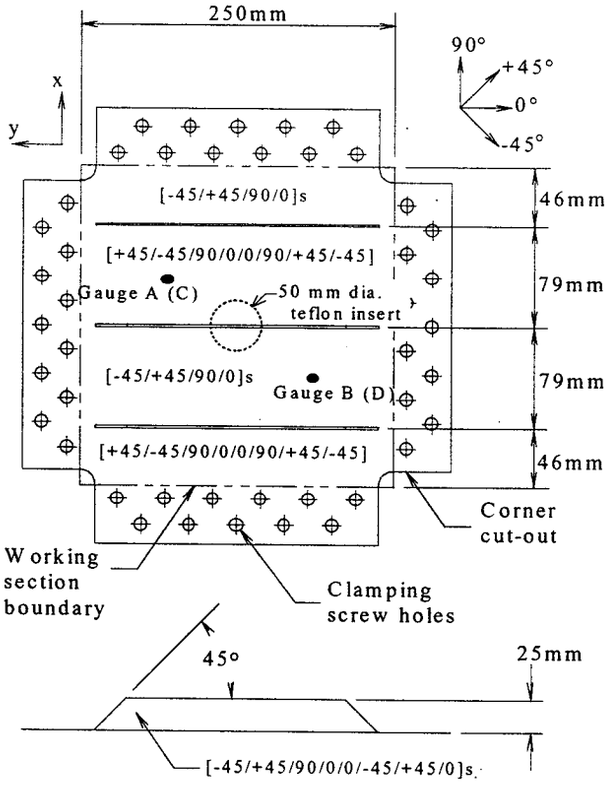

FIGURE 1 - Three-blade-stiffened panel dimensions, lay-up and strain gauge locations

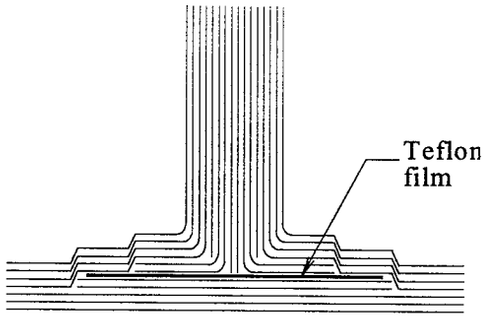

FIGURE 2 - Location of the teflon insert under the centre stiffener

TABLE 1 - Properties of T300/914C uni-directional pre-impregnated carbon epoxy tape

Property	Value
Longitudinal Modulus, E_1	130.0 GPa
Transverse Modulus, E_2	4.65 GPa
In-Plane Shear Modulus, G_{12}	4.65 GPa
Poisson's Ratio, ν_{12}	0.3
Ply Thickness	0.127 mm
Longitudinal Tension Ultimate Strain, X_T	9230 με
Longitudinal Compression Ultimate Strain, X_C	7692 με
Transverse Tension Ultimate Strain, Y_T	10750 με
Transverse Compression Ultimate Strain, Y_C	25810 με
In-plane Shear Ultimate Strain, S	13980 μγ

A uniaxial tensile load was applied diagonally through the top and bottom pins using a servo-hydraulic universal testing machine in displacement control mode. The load was applied in the direction of the -45° fibres of the panels; this represents the applied load and has been converted to shear flow throughout this paper. A data acquisition system was used to record the load, stroke, strains and out-of-plane displacement continuously during testing. When using moiré interferometry, the tests were paused at various load levels to photograph the buckled patterns.

TEST RESULTS

Global Behaviour

The test results showed that the presence of the delamination had a great influence over the behaviour of the panels. Panels without inserts buckled at an applied mean load of 31 kN (equivalent to a shear flow of 88 N/mm) and the delamination reduced this to a load of 28 kN (79 N/mm). One of the buckle peaks extended into the delaminated region shortly after buckling. Typical strain gauge output from back-to-back rosettes A and C is presented in Figure 3, where buckling is shown by bifurcation of the back-to-back strains.

Failure was first indicated by a significant crack at a load of 38 kN (107 N/mm) while sudden and unsteady delamination growth was observed at a load of 48 kN (136 N/mm). The resulting delaminated region can be seen in Figure 4. Following these events, the growth stabilised and load continued to be carried up to approximately 60 kN (170 N/mm) when significant fibre breakage occurred.

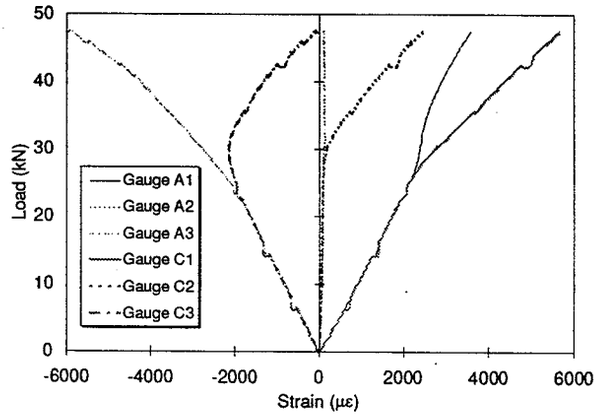

FIGURE 3 - Typical back-to-back strain output at strain gauge rosettes A and C

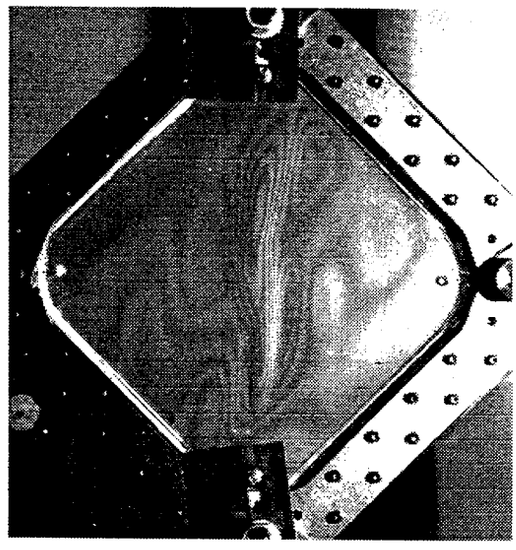

FIGURE 4 - Buckled region shown by moiré fringes at 50 kN following delamination growth

Through-transmission and pulse-echo ultrasonic C-scans performed following testing showed that the delamination had grown from the central circular area across the tension diagonal of the panel. It had been arrested only by the clamping of the test fixture. The resultant delaminated region at 55 kN (156 N/mm) is shown in Figure 5. The delamination showed several key differences between the symmetric and unsymmetric bays of the panel. Firstly, the delamination was significantly narrower in the unsymmetric bay. Secondly,

the delamination occurred primarily along the 0/90 interface on the stiffener side of the laminate in the symmetric bay while along the 0/90 interface on the skin side of the laminate in the unsymmetric bay.

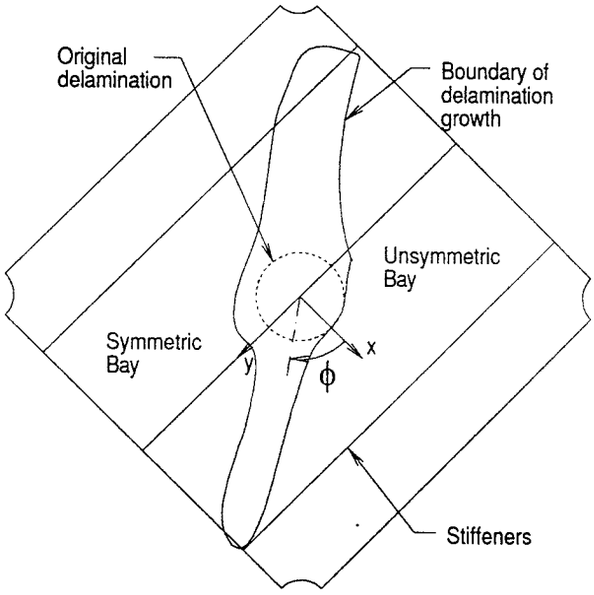

FIGURE 5 - Delaminated region following testing to 55 kN (also showing sign convention)

Fractography

A fractographic study, using a scanning electron microscope (SEM), was performed on the fracture surface surrounding the artificial delamination. This showed that a intricate and varied fracture occurred, complicated by the differing ply orientations and the presence of local ply build-ups, which can introduce local stress concentrations. In addition, characteristics of the fracture showed differences between the symmetric and unsymmetric bays, as shown in Figure 6.

The SEM fractographs of Figure 6 provide some information on the mode of fracture experienced and the direction of the principal stress, but little information on the direction of delamination propagation.[8] In both cases, the relatively clean fracture surface is indicative of a peeling (Mode I) failure. However, the presence of some "cusps" indicates a shearing type component typical of Modes II and III.[9] The spacing of the cusps indicates that the Mode I component was dominant. Fractography also showed the presence of a resin rich region at the end on the teflon film used to create the artificial delamination which could have a significant influence on the fracture initiation behaviour.

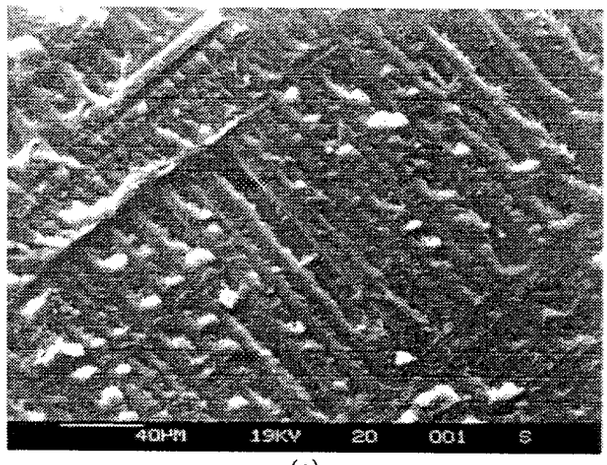

(a)

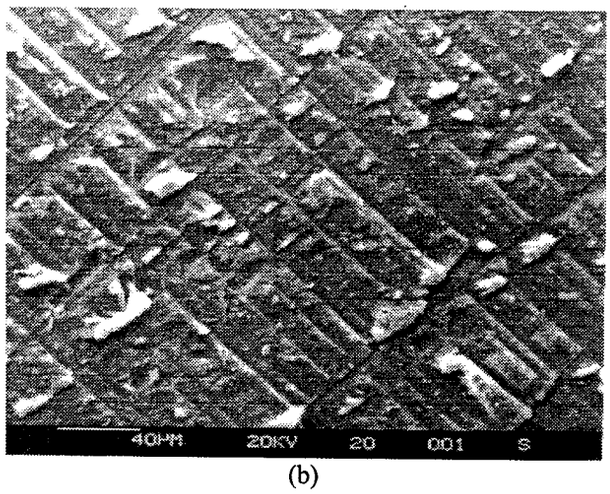

(b)

FIGURE 6 - SEM fractographs showing the typical fracture surface in the (a) symmetric and (b) unsymmetric bays near the edge of the artificial delamination. (Growth direction was left to right)

FRACTURE MECHANICS THEORY

The tests showed that a defect of this type resulted in sudden delamination growth. While analytical methods have been used to determine closed form solutions for the prediction of the effect of delaminations for some simple configurations, the complex behaviour of a postbuckling panel necessitated a numerical approach. A variety of methods exist by which fracture mechanics parameters can be determined from numerical analysis results. Typical parameters that can be used include strain energy release rates, *J*-integrals and stress intensity factors. Strain energy release rate, *G*, is a common approach used in the study of delamination growth in composites and is defined as:

$$G = \frac{dU}{da} \qquad (1)$$

where U is the total strain energy of the structure and a is the incremental crack length. A number of methods have been proposed based on the strain energy release rate which enable separation of the Mode I, II and III components. One such method is the virtual crack closure (VCC) technique which is based on the assumption that the energy required to make the crack grow a infinitesimal amount, Δ, is equal to the energy required to close the crack by the same amount. For a three-dimensional problem, a typical formulation of the strain energy release rates for a crack in the x-y plane growing in the x-direction separated into Modes I, II and III is given as follows:

$$G_I = \lim_{\Delta\to 0}\left\{\frac{1}{2\Delta\delta y}\int_y^{y+\delta y}\left[\int_0^{\Delta}\sigma_z(x,y,0)w(x-\Delta,y,0)dx\right]dy\right\}$$
$$G_{II} = \lim_{\Delta\to 0}\left\{\frac{1}{2\Delta\delta y}\int_y^{y+\delta y}\left[\int_0^{\Delta}\sigma_{xz}(x,y,0)u(x-\Delta,y,0)dx\right]dy\right\} \quad (2)$$
$$G_{III} = \lim_{\Delta\to 0}\left\{\frac{1}{2\Delta\delta y}\int_y^{y+\delta y}\left[\int_0^{\Delta}\sigma_{yz}(x,y,0)v(x-\Delta,y,0)dx\right]dy\right\}$$

where u, v and w are the crack sliding, shearing and opening displacements respectively, and δ_y is the width of the crack front over which crack closure occurs and σ_z, σ_{xz} and σ_{yz} are the normal and shear stresses on the crack plane ahead of the crack front.

This approach has been used for 3-D analyses where 8- or 20-noded brick elements were used.[10] For the analysis of composite materials, it is common to use at least one layer of brick elements for each ply of the laminate. Coupled with the limit of the aspect ratio of elements of approximately eight, this modelling approach is not feasible for the postbuckling analysis proposed due to the large number of elements required. Thus, a method in which the VCC technique can be applied to a plate element model is necessary. Such a method was developed by Wang and Raju[11] to investigate the effect of debonds between the stiffener and skin of both composite and metallic structures. While the method was derived for both four and nine-noded shell elements, only the four-noded version will be detailed in this study. It was demonstrated that this method could accurately determine strain energy release rates using 2-D shell elements.[11]

The geometry of a typical problem is shown in Figure 7. The technique uses two layers of shell elements to represent the delaminated region. The nodes of all elements are located on the plane of the delamination while the elements are offset by an amount equal to half their thickness. The double layer of elements is extended past the crack front into the non-delaminated region. This approach is useful when examining the effect of delamination growth as the position of the crack front can be easily altered. In the non-delaminated region, the degrees-of-freedom of corresponding nodes of the two surfaces were joined using multi-point constraints. Wang and Raju[11] found that joining only the translational degrees of freedom produced results most consistent with an equivalent single plate. In the delaminated region, gap elements were implemented to prevent the two layers of shell elements from passing through one another.

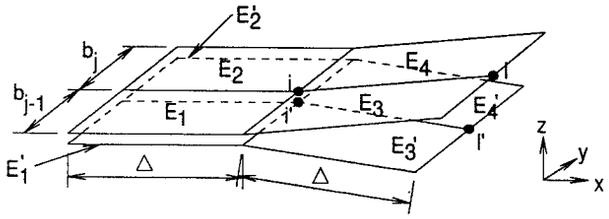

FIGURE 7 - Geometry of the crack front region using four-noded shell elements

For the 2-D problem shown in Figure 7, Equation 3 can be rewritten in terms of the forces (F_{xi}, F_{yi} and F_{zi}) and moments at the crack tip nodes and the displacements and rotations of the nodes immediately behind of the crack tip. As only the translational degrees-of-freedom are joined using MPC's, the moment terms drop out and the equations for strain energy release rate become:

$$G_I = -\frac{1}{2\Delta B_i}\left[F_{z_i}(w_i - w_{i'})\right]$$
$$G_{II} = -\frac{1}{2\Delta B_i}\left[F_{x_i}(u_i - u_{i'})\right] \quad (3)$$
$$G_{III} = -\frac{1}{2\Delta B_i}\left[F_{y_i}(v_i - v_{i'})\right]$$

where $B_i = \frac{1}{2}\left[b_{j-1} + b_j\right]$

FINITE ELEMENT (FE) MODELLING

Model Details

An FE model of an undamaged stiffened panel has been developed by the authors and was shown to accurately represent the behaviour in the postbuckling regime.[7] This model was modified to include the central delamination, as shown in Figure 8. To provide suitable resolution, the mesh was refined towards the delamination front. The elements at the crack front were approximately 1.0 mm wide (in the circumferential direction) by 0.5 mm deep (in the radial direction). The model consisted of approximately 6000 four-noded shell elements. The analysis was conducted using MSC/NASTRAN V70 on an IBM/RS6000 Model 3AT workstation.

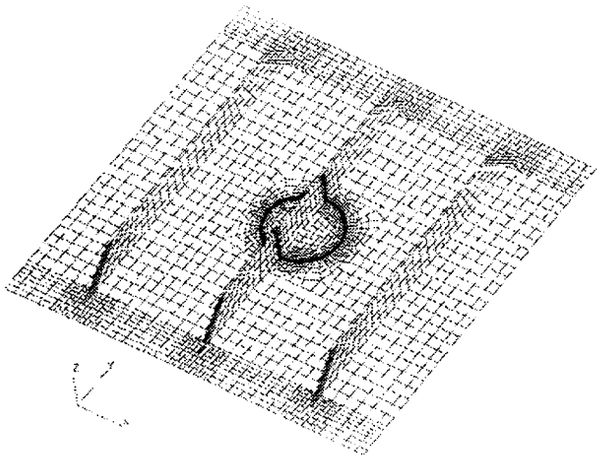

FIGURE 8 - Finite element model containing the delamination

To satisfy the requirements of the VCC technique, the FE mesh around the delamination had to be carefully constructed. All elements around the crack front were required to be perpendicular to the crack front. As the crack front was circular, it was assumed that the average width, Δ, of the elements immediately before and after the crack front would be approximately equal provided sufficient elements were used. The meshing was complicated by the ply build-ups around the stiffener base and it was necessary to slightly alter the location of these build-ups, as shown in Figure 9, to ensure that the elements at the crack front remained perpendicular to the crack front. These ply build-ups did result in some meshing problems with a small number of elements becoming skewed or having high aspect ratios.

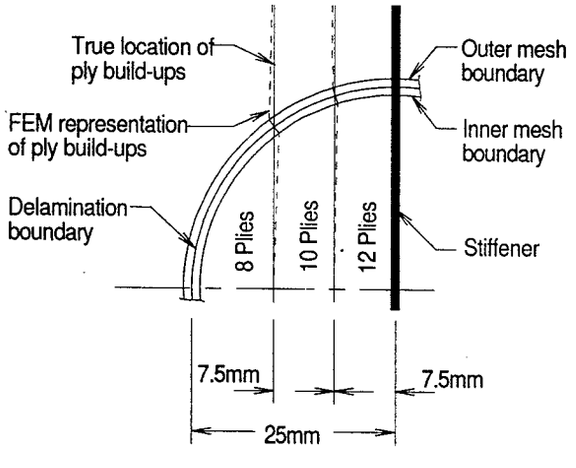

FIGURE 9 - Detail of one quadrant in the central region of the panel showing the location of the actual and assumed ply build-ups

The double layer of shell elements used to represent the delamination only extended 1 mm past the delamination front. This distance was kept to a minimum since the stiffness in the overlapping elements which are joined using MPC's is not a perfect representation of a single element. The bending stiffness of the elements is critical in a postbuckling analysis and a large overlapping region could unduly influence the postbuckling deformation.

The analysis was computationally demanding due in part to the large number of elements resulting from the necessarily detailed model. Additionally, the presence of gap elements increased the computational demands. A postbuckling analysis requires incremental load steps with iterations at each load step to arrive at the solution and the presence of gap elements required additional iterations to determine the position of the gaps (open or closed).

Implementation of the VCC Technique

The displacements and forces from the FE analysis were transformed from the global coordinate system to the local coordinate system at each node on the delamination front. This local coordinate system was aligned with both the local direction of the crack front and the plane of the delamination in its deformed position, where x-y-z are the global coordinates (Figures 1 and 5) and x_L-y_L-z_L are defined as the local coordinates. The angles α_x, α_y and α_z are defined as the transformation angles between the global and local coordinate frames. These angles consist of two parts, the first of which is due to the position of the nodes on the delamination front which involves a simple rotation about the global z-axis, ϕ. The other part is due to deformation of the panel under load, which may involve significant rotations about all three axes (θ_x, θ_y, θ_z) given the postbuckling nature of the problem. These rotations were determined by averaging the nodal rotations from the pair of nodes, i and i', located at the delamination front. Thus, the three components can be defined as:

$$\alpha_x = \frac{\left(\theta_{x_i} + \theta_{x_{i'}}\right)}{2}$$
$$\alpha_y = \frac{\left(\theta_{y_i} + \theta_{y_{i'}}\right)}{2} \qquad (4)$$
$$\alpha_z = \phi + \frac{\left(\theta_{z_i} + \theta_{z_{i'}}\right)}{2}$$

The transformation matrix $[T]$ is defined as:

$$\{u_L\} = [T]\{u\} \qquad (5)$$

and

$$\{F_L\} = [T]\{F\} \qquad (6)$$

where $\{u_L\}$ and $\{F_L\}$ are the transformed nodal displacements and forces respectively. Results from the analysis show that α_x and α_y are small, so $\sin\alpha_x$ and $\sin\alpha_y$ tend to zero. Thus, it can be shown that:

$$[T]=\begin{bmatrix} \cos\alpha_z \cos\alpha_y & \sin\alpha_z \cos\alpha_x & 0 \\ \sin\alpha_z \cos\alpha_y & \cos\alpha_z \cos\alpha_x & 0 \\ 0 & 0 & \cos\alpha_x \cos\alpha_y \end{bmatrix} \quad (7)$$

Global Analysis Results

The buckling load predicted by the FE analysis agreed with the experimental result. The predicted buckling mode shape was also predicted very well when compared with the moiré interferometry results. A typical comparison of the back-to-back shear strains is presented in Figure 10, which confirms the accuracy of the FE prediction. Some deviation of the predicted and experimental strains is noted at loads greater than 40 kN which can be attributed to the initiation of damage. During testing, a cracking was first heard at 38 kN.

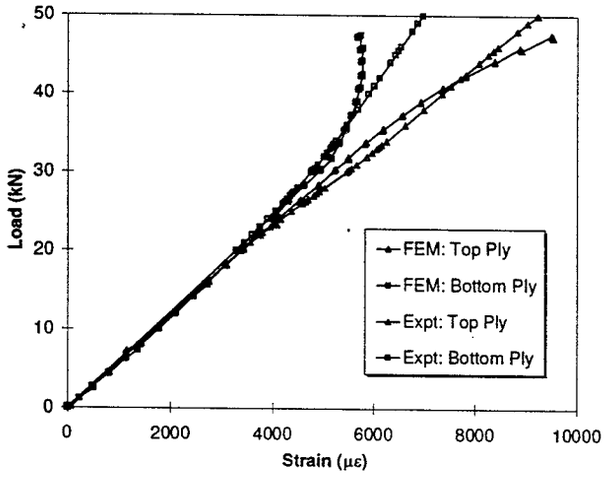

FIGURE 10 - Comparison of experimental and predicted back-to-back shear strains at strains gauges A and C

Fracture Results

The strain energy release rate results showed there was a large variation in G around the circumference of the delamination. In addition, the contribution of the various modes changed significantly with radial position. The variation in the three components of G around the delamination at 50 kN load is presented in Figure 11. This corresponds to the load at which delamination growth was observed. The dominant features are two peaks in G_{III} located at -120° and 70°. Peaks in G_I occurred at -110° and 65° while G_{II} peaks occurred at -30° and 140°. The positions of these peaks were relatively independent of load following buckling. Figure 11 also demonstrates the complicated distribution in the components of G around the delamination. This is due to the global shear buckling of the panel, local buckling of the sub-laminate and also the complicated lay-up of the panel which consists of symmetric and unsymmetric bays and well as local ply build-ups.

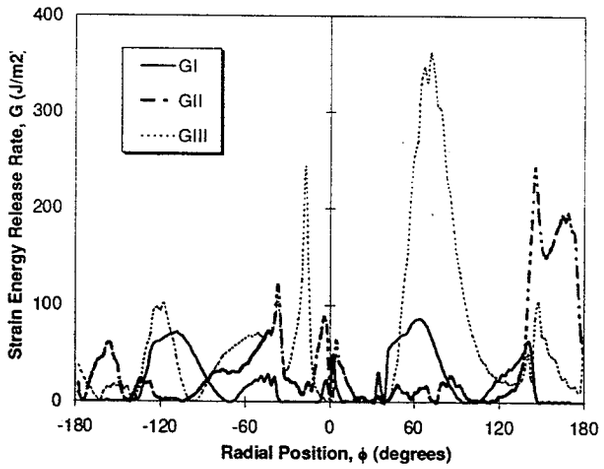

FIGURE 11 - Predicted variation in strain energy release rate around the delamination at 48 kN

The variation of maximum strain energy release rate around the delamination with load is shown in Figure 12. The strain energy release rate increases dramatically when the panel begins to buckle. The process of buckling allows the delamination to open up thus increasing the likelihood of delamination growth.

Prediction of the load at which delamination growth will initiate requires suitable fracture mechanics parameters for the material; figures from the literature for the critical strain energy release rates in Modes I and II are quoted in Table 2. Critical Mode III fracture toughness, which is usually much greater than Mode II, is not included as the data are questionable. The fracture toughness values quoted in Table 2 can vary significantly depending on the source, data reduction scheme, laminate and the ply orientations. The fact that the local orientation of the plies varies with circumferential position complicates the issue further.

The results from the analysis clearly predict that a mixed-mode fracture will occur. However, the critical value of strain energy release rate in Mode II is approximately three times that in Mode I. Likewise, the Mode III critical value of strain energy release rate is typical quoted to be an order of magnitude greater than

the Mode I value.[13] Thus, the results indicate that G_I will reach its critical value prior to the other modes and this mode will drive the delamination process. The location of the two peaks in G_I correspond to the locations where delamination growth occurred during testing. This Mode I component is a result of the buckling and opening up of the sub-laminates in the artificial delamination. The prediction of a Mode I dominated fracture is supported by the SEM fractography results.

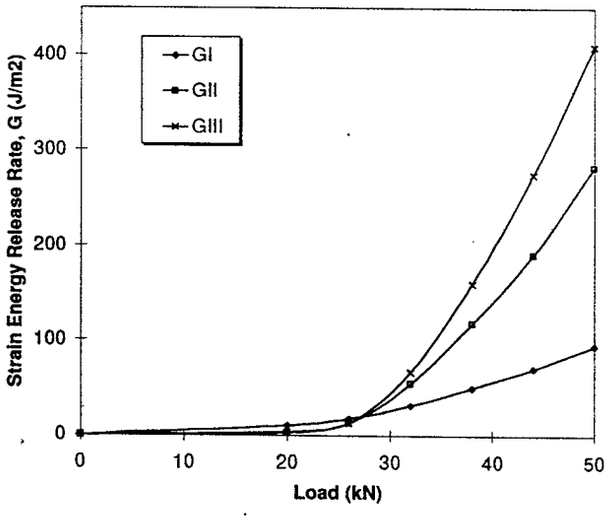

FIGURE 12 - Predicted variation in maximum strain energy release rate components around the delamination with load

TABLE 2 - Typical critical strain energy release rates for T300/914C unidirectional carbon epoxy tape[12]

Mode I - G_{Ic}	150 J/m^2
Mode II - G_{IIc}	430 J/m^2

CONCLUSIONS

The postbuckling performance of three-blade-stiffened carbon fibre/epoxy shear panels containing 50 mm diameter artificial delaminations located under the central stiffener has been investigated. Static tests were conducted in a "picture frame" shear fixture. During static testing, buckling initiated at 28 kN (79 N/mm) while the panels suffered delamination growth at 48 kN (136 N/mm). Ultimate failure in the form of extensive fibre breakage occurred at approximately 60 kN (170 N/mm).

An analysis technique to determine the effect of the artificial delamination on the panel performance was proposed. This used the VCC technique to determine the strain energy release rate around the circumference of the imbedded delamination. The VCC technique was applied to the results from a geometric nonlinear finite element analysis using two-dimensional plate elements. The predicted location and mode of delamination growth was shown to agree well with experimental results. Further work is required to be able to predict the actual failure load due to the mixed mode failure experienced.

REFERENCES

1. Weller, T. and Singer, J., "Durability of Stiffened Composite Panels Under Repeated Buckling," *International Journal of Solids and Structures*, Vol. 26, No. 9-10, 1990, pp. 1037-1069.

2. Agarwal, B.L., "Postbuckling Behavior of Composite Shear Webs," *AIAA Journal*, Vol. 19, No. 7, July 1981, pp. 933-939.

3. Panhwar, N.M., Thomson, R.S. and Scott, M.L. "Durability of Postbuckling Fibre Composite Panels Under Shear", *Proc. Fifth Australian Aeronautical Conference*, Melbourne, Victoria, Australia, September 13-15, 1993, Vol. 1, pp. 75-80.

4. Wiggenraad, J.F.M., Aoki, R., Gadke, M., Greenhalgh, E., Hachenberg, D., Wolf, K. and Bubl, R., "Damage Propagation in Composite Structural Elements - Analysis and Experiments on Structures," *Composite Structures*, Vol.36, 1996, pp. 173-186.

5. Gadke, M., Geier, B., Goetting, H., Klein, H., Rohwer, K., and Zimmermann, R., "Damage Influence on the Buckling Load of CFRP Stringer-stiffened Panels," *Composite Structures*, Vol. 36, 1996, pp. 249-275.

6. Greenhalgh, E., Bishop, S.M., Bray, D., Hughes, D., Lahiff, S. and Millson, B., "Characterisation of Impact Damage in Skin-Stringer Composite Structures," *Composite Structures*, Vol. 36, 1996, pp. 187-207.

7. Thomson, R.S. and Scott, M.L., "Testing and Analysis of Thin Stiffened Carbon Epoxy Shear Panels," *Proc. Second Pacific International Conference on Aerospace Science and Technology - Sixth Australian Aeronautical Conference*, Melbourne, Victoria, Australia, March 20-23, 1995, Vol. 2, pp. 655-662.

8. Bascom, W.D. and Gweon, S.Y., "Fractography and Failure Mechanisms of Carbon-Reinforced Composite Materials," In: *Fractography and*

Failure Mechanisms of Polymers and Composites, Roulin-Moloney, A.C. (Ed), Elsevier, 1990.

9. Purslow, D., "Matrix Fractography of Fibre-reinforced Epoxy Composites," *Composites*, Vol. 17, No. 4, 1986, pp. 289-303.

10. Whitcomb, J.D., "Three-Dimensional Analysis of a Postbuckled Embedded Delamination," *Journal of Composite Materials*, Vol. 23, 1989, pp. 862-889.

11. Wang, J.T. and Raju, I.S., "Strain Energy Release Rate Formulae for Skin-Stiffener Debond Modeled with Plate Elements," *Engineering Fracture Mechanics*, Vol. 54, No. 2, 1996, pp. 211-228.

12. Backhouse, R., Blakeman, C. and Irving, P.E., "Mechanisms of Toughness Enhancement in Carbon Fibre Non-crimp Fabrics," *Proc. of the Third International Conference on Deformation and Fracture of Composites*, March 27-29, 1995, Guildford, UK, pp. 307-316.

13. Donaldson, S.L., "Interlaminar Fracture Due to Tearing (Mode III)," *Proc. ICCM VI and ECCM II*, London 1987, Elsevier, Vol. 3, pp. 274-283.